Performance Characteristics and Metrics for Intra-Pulse Radar-Embedded Communication

Shannon D. Blunt, Justin G. Metcalf, Casey R. Biggs, and Erik Perrins,

Abstract

Low probability of intercept (LPI) communication generally relies on the presence of noise to obfuscate a covert signal through the use of spectral spreading or hopping. In contrast, this paper addresses the use of ambient interference from other man-made emissions as a means to mask the presence of covert communication. Specifically, the high power, wide bandwidth, and repeating structure of pulsed radar systems provide an advantageous framework within which to embed a communication signal. The operating paradigm considered here is that of an RF tag/transponder that is illuminated by the radar and intends to covertly communicate with the radar or some other desired receiver while being masked by the ambient radar backscatter to avoid detection by an intercept receiver. Communication takes place on an intra-pulse (or individual pulse) basis to maximize the data rate. The impact of multipath, and its exploitation using time reversal to achieve spatio-temporal focusing, is considered. The processing gain for the destination receiver and intercept receiver are derived analytically and subsequently used to optimize the parameterization of communication symbol design.

Index Terms

LPI communications, pulsed radar, RF tag/transponder, interference cancellation

I. Introduction

We consider the design trade-offs and performance metrics for an intra-pulse radar-embedded communication system [1]. In such a system, a radar (which may or may not be cooperative) illuminates a region that contains an RF tag/transponder [2] [3](for simplicity, henceforth referred to as the ”tag”). The tag may operate in a purely passive mode, harvesting energy from the

The authors are with the Electrical Engineering & Computer Science Dept., University of Kansas, Lawrence, KS.

This work was supported by the Air Force Office of Scientific Research.

radar illumination, or it may be an active transmitter that is triggered by the incident radar illumination. The tag embeds, either through modulation of the incident illumination or by triggered transmission, one of K communication symbols into the ambient backscatter induced by the radar reflections. By operating on an individual pulse (or intra-pulse) basis the embedded communication data-rate is on the order of the pulse repetition frequency (PRF) of the radar (typical values of which are 1-10 kHz).

Covert communication is traditionally performed via the spread spectrum paradigm where the signal is either spread or rapidly hopped in frequency to distribute the signal energy so that it can remain hidden in noise. One limitation of this approach is that to enable effective communication (*i.e.* low bit error rate (BER)) with a distant receiver the required transmit signal power may not have a low probability of intercept (LPI) with respect to a nearby intercept receiver since it is the signal-to-noise ratio (SNR) that dictates both of these conflicting performance metrics [4]. In contrast, we consider the case in which an additional interference source is present that may be advantageously exploited to mask the covert communication signal. Generally speaking, the obvious choice for an interference source is one that is already present, such as radar emissions [5], [6], [7] or existing communications infrastructure [8]. The selection of proper covert communication symbols is thus dependent upon the nature of the masking interference and may possibly be determined through observation of the current interference emissions or through available knowledge of signaling protocols and standards used by the interference source.

The notion of incorporating information into backscatter emissions can be traced back to Stockman in the 1940's [9]. The use of radar emissions for this purpose can be broadly characterized as forms of ”inter-pulse” communication in which a single symbol is inserted for each coherent processing interval (CPI) of the radar that may consist of 10's to even 1000's of radar pulses. Given a radar PRF on the order of a few kHz, the resulting data rate in the neighborhood of 1-100 bps is obviously quite low. That said, when used to provide passive identify friend or foe (IFF) functionality in conjunction with an imaging radar modality such as synthetic aperture radar (SAR), these inter-pulse methods can be used to spatially track friendly assets thus reducing instances of battlefield ”friendly fire”.

Whereas a communication symbol for the *inter*-pulse framework consists of a sequence of phase shifts across numerous pulses in a CPI (akin to Doppler phase shifts introduced by relative motion), the *intra*-pulse approach recently proposed in [1] embeds an independent covert symbol for each individual radar pulse. For example, Fig. 1 provides a notional illustration where the symbol generated by the tag is hidden among the ambient radar scattering while being sufficiently identifiable by an intended receiver that possesses prior knowledge of the symbol characteristics.

To effectively hide the covert symbol (*i.e.* to prevent it from being easily discriminated from ambient scattering) requires that the symbol be in some way related to the phase or frequency sequence that is modulated onto the radar pulse (otherwise known as the radar waveform) so as to achieve a prescribed range resolution via pulse compression [10], [11]. The trade-off in the design of covert symbols is that they must be sufficiently different from the ambient random scattering (i.e. ”clutter”) to maintain acceptable BER performance at the intended destination receiver while also being sufficiently similar to the clutter to prevent detection by an intercept receiver. Thus it is also necessary for the destination receiver to employ some form of interference cancellation to effectively extract the embedded symbol from the masking interference.

The design of the ”constellation” of K intra-pulse covert symbols based on the incident radar waveform was the focus of [1]. This paper examines the impact of multipath on symbol design to assess the potential for symbol mismatch between the tag and the intended receiver. It is also shown that, due to the intrinsic two-way communication path for intra-pulse radar-embedded communication, if the tag intends to communicate with the illuminating radar the use of time reversal [12] can be naturally incorporated by estimating the multipath at the tag and assuming reciprocity of the transmission medium. Additionally, the decision process for estimation of the embedded symbol at the destination receiver is cast as a two-stage detector so as to minimize the detection of false symbols and as a way for the destination receiver to self-synchronize without the need for prior cueing. Finally, the processing gains for the destination receiver and a hypothetical intercept receiver are analytically derived and it is shown that their ratio provides a “gain advantage” design metric that can be used for symbol design. Performance is assessed in terms of BER and probability of intercept.

II. SIGNAL MODELS FOR EMBEDDED COMMUNICATION

The process of embedding a covert communication signal into radar backscatter on an intra-pulse basis can be viewed as two separate components: 1) the generation of the set of K symbols depending upon the ambient radar clutter and 2) the recovery of the embedded signal from the noise and the higher power clutter interference. The first component can be viewed as a *forward* *link* while the second can be viewed as a *reverse link*. As such it is appropriate to consider the signal model for each component separately.

A. Incident Radar Illumination (Forward Link)

For a transmitted radar pulse having pulsewidth T the modulation on the pulse is defined as the waveform $s(t)$. The incident radar illumination can be generically expressed as

$$\widetilde{s}(t) \;=\; \alpha_{\mathrm{R}\bullet}\left[s(t) * h_{\mathrm{R}\bullet}(t)\right] + u(t) \tag{1}$$

where $\alpha_{\mathrm{R}\bullet}$ subsumes the strength of the radar transmission and the one-way (forward link) attenuation to some given location, $h_{\mathrm{R}\bullet}(t)$ is the continuous multipath channel between the radar and some given location (including direct path and path-induced dispersive effects), $*$ is convolution, and $u(t)$ is additive white Gaussian noise (AWGN). Specifically, we shall denote $h_{\mathrm{RT}}(t)$ as the multipath between the radar and tag, $h_{\mathrm{RD}}(t)$ as the multipath between the radar and the intended "destination receiver" (for the embedded communication signal in the reverse link), and $h_{\mathrm{RI}}(t)$ as the multipath between the radar and an intercept receiver. If the radar is to be the destination receiver we define its "incident" illumination as $\widetilde{s}(t) = s(t)$ since the radar has access to the actual transmitted radar waveform.

Given the incident illumination $\widetilde{s}(t)$ that may be corrupted by multipath, both the tag and destination receiver must determine the set of K symbols in such a way that is robust to disparities between the respective multipath channels (due to different incident locations) as well as possible differences induced by receiver hardware (*e.g.* sampling rate differences, synchronization issues, etc). In Section III-A a symbol design technique is presented that provides this robustness. Note that, because most radar applications involve the repetition of the same waveform for numerous pulses in a CPI, this design process need only be performed when the waveform changes.

B. Radar Backscatter with Embedded Symbol (Reverse Link)

For the time interval in which the embedded symbol and ambient radar backscatter (clutter) are incident at a given receiver (either destination or intercept), the reverse link signal model can be expressed as

$$y(t) = s(t) * x(t) \;+\; \alpha_{\mathrm{T}\bullet}\left[c_k(t) * h_{\mathrm{T}\bullet}(t)\right] \;+\; u(t) \tag{2}$$

where $x(t)$ is arbitrary ambient radar scattering (t here corresponds to the range delay with respect to the radar), $c_k(t)$ is the k^{th} communication symbol, $\alpha_{\text{T}\bullet}$ subsumes the transmit strength of the tag and the one-way (reverse link) attenuation, and $h_{\text{T}\bullet}(t)$ is the multipath between the tag and some given location. Specifically, we shall denote $h_{\text{TD}}(t)$ as the multipath between the tag and the destination receiver (which could be the radar), and $h_{\text{TI}}(t)$ as the multipath between the tag and an intercept receiver.

By setting the tag-generated signal power to be much less than the average clutter power in the surrounding region (or by the introduction of artificial clutter through the use of a digital RF memory (DRFM) device [13]), a well-designed symbol $c_k(t)$ will be indistinguishable from the clutter. Conversely, given the set of K possible symbols at the destination receiver, coherent integration combined with interference cancellation (of the clutter) can still yield acceptable covert communication performance. The receive filtering and subsequent symbol detection are discussed in Section IV-A. As an example, Figure 2 illustrates the overall signal model (including forward and reverse links) for the case where the tag communicates with the illuminating radar.

III. Symbol Design in Multipath

To maximally leverage the masking interference of the radar clutter the embedded symbols are made to be functionally dependent upon the illuminating radar waveform such that the symbols are inseparable from the backscatter without *a priori* knowledge. Of course this means that both the tag and the destination receiver must obtain the symbols separately which could lead to mismatch effects. It was previously shown [1] that a mismatch-robust approach for symbol design is to construct the symbols according to the dominant subspace of a correlation matrix that models the ambient radar scattering. Here we consider the mismatch-inducing impact of multipath due to its inherent variability according to spatial location.

A. Robustness to Multipath

Given the incident radar illumination $\widetilde{s}(t)$ of (1) at some arbitrary location, let N be the number of samples required to sufficiently represent the incident radar illumination according to the Nyquist criterion for the half-power bandwidth (thus N is the time-bandwidth product) and M be the additional factor by which the waveform is over-sampled (to facilitate sufficient degrees of freedom for symbol design). Thus a discretized version of the incident radar illumination can be expressed as $\widetilde{\mathbf{s}} = \begin{bmatrix} \widetilde{s}_0 & \widetilde{s}_1 & \cdots & \widetilde{s}_{NM-1} \end{bmatrix}^T$. Based on this discretized version of the radar illumination the ambient scattering in the surrounding area can be modeled as $\widetilde{\mathbf{S}}\mathbf{x}$ where $\mathbf{x}$ is a vector of arbitrary random scattering coefficients and

$$\widetilde{\mathbf{S}} = \begin{bmatrix} \widetilde{s}_{NM-1} & \widetilde{s}_{NM-2} & \cdots & \widetilde{s}_0 & 0 & \cdots & 0 \\ 0 & \widetilde{s}_{NM-1} & & \widetilde{s}_1 & \widetilde{s}_0 & & 0 \\ \vdots & & \ddots & \vdots & \vdots & \ddots & \\ 0 & 0 & & \widetilde{s}_{NM-1} & \widetilde{s}_{NM-2} & \cdots & \widetilde{s}_0 \end{bmatrix} \tag{3}$$

characterizes the convolution of the waveform with the local scattering. Variations in multipath need not be considered due to the associative property of linear systems where

$$\widetilde{s}(t) * x(t) \;=\; s(t) * h(t) * x(t) \;=\; s(t) * \widetilde{x}(t) \tag{4}$$

and $\widetilde{x}(t)$ can be viewed as another arbitrary random scattering profile.

Assuming that the clutter is uncorrelated (*i.e.* $E\big[\mathbf{x}\mathbf{x}^H\big] = \sigma_x^2\,\mathbf{I}$, for σ_x^2 the average clutter power), a power-normalized $NM \times NM$ correlation matrix for the ambient scattering and its subsequent eigen-decomposition can be obtained as

$$\frac{1}{\sigma_x^2} E\left[\left(\widetilde{\mathbf{S}}\mathbf{x}\right)\left(\widetilde{\mathbf{S}}\mathbf{x}\right)^H\right] = \widetilde{\mathbf{S}}\widetilde{\mathbf{S}}^H = \mathbf{V}\boldsymbol{\Lambda}\mathbf{V}^H \tag{5}$$

where $\mathbf{V}$ is the set of NM eigenvectors, $\boldsymbol{\Lambda}$ contains the NM eigenvalues on the diagonal (with $\lambda_1 \geq \lambda_2 \geq \cdots \geq \lambda_{NM}$), and $(\cdot)^H$ is the Hermitian operation. We shall denote the set of eigenvectors associated with the first m eigenvalues as forming the dominant subspace $\mathbf{V}_{\text{D}}$ and the remaining $NM - m$ eigenvectors as forming the non-dominant subspace $\mathbf{V}_{\text{ND}}$. A design metric for the determination of m is derived in Section V.

Given a set of seed vectors $\mathbf{b}_k$ for $k = 1, 2, \cdots, K$ known to both the tag and destination receiver, the discretized set of symbols $\mathbf{c}_k$ can be obtained by the projection operation

$$\mathbf{c}_k = \mathbf{P}\mathbf{b}_k \tag{6}$$

where

$$\mathbf{P} = \mathbf{I} - \mathbf{V}_{\text{D}}\mathbf{V}_{\text{D}}^H = \mathbf{V}_{\text{ND}}\mathbf{V}_{\text{ND}}^H \tag{7}$$

such that the K symbols are projected onto the non-dominant subspace. To demonstrate that the symbol structure is preserved despite differences in multipath consider $\mathbf{c}_{k,1}$ and $\mathbf{c}_{k,2}$ formed from the projections $\mathbf{P}_1$ and $\mathbf{P}_2$ that result from distortion of the radar waveform $s(t)$ by independent multipath channels $h_1(t)$ and $h_2(t)$, respectively. The normalized correlation between the two versions of the k^{th} symbol can be defined as

$$\beta = \frac{\left|\mathbf{c}_{k,1}^H \ \mathbf{c}_{k,2}\right|^2}{\left(\mathbf{c}_{k,1}^H \ \mathbf{c}_{k,1}\right)\left(\mathbf{c}_{k,2}^H \ \mathbf{c}_{k,2}\right)} \tag{8}$$

which, by invoking the Hermitian ($\mathbf{P}^H = \mathbf{P}$) and idempotent ($\mathbf{P}\mathbf{P} = \mathbf{P}$) properties of the projection matrix, can also be expressed as

$$\beta = \frac{\left|\mathbf{b}_k^H \ \mathbf{P}_1 \ \mathbf{P}_2 \ \mathbf{b}_k\right|^2}{\left(\mathbf{b}_k^H \ \mathbf{P}_1 \ \mathbf{b}_k\right)\left(\mathbf{b}_k^H \ \mathbf{P}_2 \ \mathbf{b}_k\right)} \ , \tag{9}$$

where $0 \leq \beta \leq 1$, with $\beta = 1$ signifying no mismatch. Thus the degree of symbol mismatch due to different multipath profiles can be defined as

$$\eta = 10 \log_{10} (1 - \beta) \tag{10}$$

where the mismatch-free case would yield $\eta = -\infty$.

Using the dominant and non-dominant forms in (7) the product of projections in the numerator of (9) can be expressed as

$$\mathbf{P}_1 \ \mathbf{P}_2 = \left[\mathbf{I} - \mathbf{V}_{\text{D},1}\mathbf{V}_{\text{D},1}^H\right]\left[\mathbf{V}_{\text{ND},2}\mathbf{V}_{\text{ND},2}^H\right] = \mathbf{V}_{\text{ND},2}\mathbf{V}_{\text{ND},2}^H - \mathbf{V}_{\text{D},1}\mathbf{V}_{\text{D},1}^H\mathbf{V}_{\text{ND},2}\mathbf{V}_{\text{ND},2}^H \ . \tag{11}$$

If the dominant and non-dominant subspaces are preserved for two different multipath profiles, then $\mathbf{V}_{\text{D},1}^H\mathbf{V}_{\text{ND},2} = \mathbf{0}_{N \times N(M-1)}$ in the last term such that (11) simplifies to $\mathbf{V}_{\text{ND},2}\mathbf{V}_{\text{ND},2}^H = \mathbf{P}_2$. Again invoking the idempotent property, the result that $\mathbf{P}_1 \ \mathbf{P}_2 = \mathbf{P}_2$ implies that $\mathbf{P}_1 = \mathbf{P}_2$ and hence no mismatch exists. Thus robustness to symbol mismatch for arbitrary multipath profiles can be maintained by preserving the separation between the dominant and non-dominant subspaces. Furthermore, arbitrary transformations of the subspace, as long as they preserve the separation, will have no effect on symbol mismatch.

As an example, consider a typical linear FM radar waveform [10] with $N = 100$ that is over-sampled by $M = 2$. For each of 1000 independent trials, two random multipath profiles are convolved with the waveform. Each multipath profile consists of 1 direct path impulse and 9 multipath impulses randomly distributed in time (via a uniform distribution over $[0, T/2]$) with each of the 10 impulses multiplied by a value drawn from a complex Gaussian distribution (to randomize amplitude and phase). For the sake of consistency each multipath-corrupted radar waveform is truncated to $NM = 200$ samples. The resulting multipath-corrupted versions of the radar waveform are used to obtain $K = 4$ symbols for the rank of the dominant subspace $\mathbf{V}_{\mathrm{D}}$ set to $m = NM/2 = 100$. For this scenario it is observed that the average value of mismatch over the set of 1000 trials and over the 4 symbols is $\eta_{\mathbf{mean}} = -9.0$ dB, with the best and worst observed mismatch values being $\eta_{\mathbf{best}} = -19.5$ dB and $\eta_{\mathbf{worst}} = -3.9$ dB, respectively. Figure 3 also illustrates $10\log_{10}\left(\left|\mathbf{V}_1^H\mathbf{V}_2\right|\right)$ averaged over the 1000 trials which provides a graphical interpretation of how the subspaces are preserved (top-left is dominant and bottom-right is non-dominant). The off-diagonal quadrants represent the average subspace leakage.

B. Exploiting Multipath via Time-Reversal

Due to the intrinsic two-way nature of this signaling scheme, if the destination receiver is the illuminating radar and under the assumption of reciprocity of the environment (i.e. $h_{\mathrm{RT}}(t) = h_{\mathrm{TR}}(t)$) and the availability of an adequate estimate of the radar-to-tag multipath, then time-reversal [12] can readily be incorporated into the symbol design. Because time-reversal provides spatio-temporal focusing as a result of correlation with the multipath channel, the resulting gain can be used to enhance detection of the embedded symbol at the radar receiver without adversely affecting LPI capability.

If the tag possesses *a priori* knowledge of the illuminating radar waveform (uncorrupted by multipath) then the radar-to-tag multipath $h_{\mathrm{RT}}(t)$ can be easily estimated at the tag using standard matched filtering such as is employed for radar pulse compression as

$$\widehat{h}_{\mathrm{RT}}(t) = s(-t) * \widetilde{s}(t). \tag{12}$$

Given the multipath estimate $\widehat{h}_{\mathrm{RT}}(t)$, it can be incorporated into the symbol design as

$$\widetilde{c}_k(t) = \widehat{h}^*_{\mathrm{RT}}(-t) * c_k(t) \tag{13}$$

where $(\cdot)^*$ is complex conjugation. Thus the received signal at the radar from (2) becomes

$$\begin{aligned} y(t) &= s(t) * x(t) + \alpha_{\mathrm{TR}}\left[\widetilde{c}_k(t) * h_{\mathrm{TR}}(t)\right] + u(t) \\ &= s(t) * x(t) + \alpha_{\mathrm{TR}}\left[c_k(t) * r_{\mathrm{TR}}(t)\right] + u(t) \end{aligned} \tag{14}$$

where $r_{\mathrm{TR}}(t) = \widehat{h}^*_{\mathrm{TR}}(-t) * h_{\mathrm{TR}}(t)$ is the autocorrelation of the multipath.

The performance benefit of time-reversal will be demonstrated in Section VI. While not addressed here, it may be possible to use blind deconvolution approaches to estimate the multipath by making the plausible assumption that the radar waveform is constant modulus and exploiting the finite time support of the incident pulse.

IV. Symbol Detection

Defining the sampled version of the reverse link received signal as $y(\ell)$ we consider if one of the K symbols can be detected for a given set of MN samples denoted as $\mathbf{y}(\ell) = \left[y(\ell) \quad y(\ell-1) \quad \cdots \quad y(\ell-NM+1)\right]^T$ within an observation interval $\gg NM$. Because the received clutter power may be orders of magnitude higher than the embedded symbol, some form of interference cancellation is required. The K receive filters for the K symbols can be defined as $\mathbf{w}_k$ for $k = 1, 2, \cdots, K$, which when applied yield $\mathbf{w}_k^H \mathbf{y}(\ell) = z_{y,k}(\ell)$. In [1] a simple metric was used to determine which symbol was present by selecting the symbol that provides the largest magnitude filtered response over the set of K filters and over the entire observation interval (where it is assumed that only one symbol is present). With respect to the new proposed detector in Figure 4, the previous detection process involved selecting the maximum value over the set $\{|z_{y,1}(\ell)|\,,\ |z_{y,2}(\ell)|\,,\ \cdots\,,\ |z_{y,K}(\ell)|\}$ for all values of ℓ in the observation interval. We denote this maximum value as $\left|z_{y,\max}^{(k)}\right|$ where (k) indicates the corresponding symbol.

The previous detector ignored the null hypothesis (symbol absent). However, the presence of large interference coupled with the difficulty of precise synchronization could lead to significant false symbol detections. To accommodate the inclusion of the null hypothesis a second stage is appended that compares the maximum value $z_{y,\max}^{(k)}$ with a threshold $\mathcal{T}$ that is determined from the other $K-1$ filtered responses $z_{y,\,j\neq k}(\ell)$ based on the logic that they provide a baseline that is calibrated to the interference-residue from which a true embedded symbol should stand out. The other time-shifted responses of $z_{y,k}(\ell)$ are excluded from the determination of $\mathcal{T}$ to avoid contamination from possible multipath-induced replicas of the k^{th} symbol. If $z_{y,\max}^{(k)} > \mathcal{T}$ then the k^{th} symbol is deemed correct, otherwise no symbol detection can be declared. Thus the goal is to determine the appropriate set of filters $\mathbf{w}_k$ and the threshold $\mathcal{T}$ that maximize the probability of detection of the correct symbol (including the "no symbol" case). The following discusses the selection of interference cancellation filters as well as the hypotheses for the two stages of the detector.

A. Receive Filtering

It is well known that the matched filter $\mathbf{w}_k = \mathbf{c}_k$ maximizes the signal-to-noise ratio (SNR) of a signal in noise. Thus in the absence of interference the only design requirement would be to minimize the correlation between the K symbols (which can be accomplished via the sequential implementation of (6) discussed in [1]). In the presence of interference the sampled received signal for the length NM interval containing the embedded symbol can be expressed as

$$\mathbf{y} = \mathbf{S}\mathbf{x} + \alpha \mathbf{c}_k + \mathbf{u} \tag{15}$$

where $\mathbf{S}$ is a matrix of delay shifts of the discretized radar waveform $\mathbf{s}$ as in (3) albeit without multipath distortion, $\mathbf{x}$ is a vector of discrete samples of random scattering, and $\mathbf{u}$ is a vector of noise samples. Thus the metric to optimize here is signal-to-interference-plus-noise ratio (SINR).

Because the structure of the interference is partially known via the matrix $\mathbf{S}$, a straightforward choice is the decorrelator [14], [15] that is obtained from maximum likelihood estimation and is employed for CDMA multiuser detection which, for the problem at hand, can be expressed as

$$\mathbf{w}_k = \left(\mathbf{S}\mathbf{S}^H + \delta \mathbf{I}\right)^{-1} \mathbf{c}_k \quad \text{for} \quad k = 1, 2, \ldots, K \tag{16}$$

where $\delta = \lambda_{m+1}$ is the largest non-dominant eigenvalue and $\mathbf{I}$ is an identity matrix. The diagonal loading term $\delta \mathbf{I}$ is included for mathematical convenience of the processing gain analysis in Section IV-C. Per (4), using a multipath-distorted $\widetilde{\mathbf{S}}$ in (16) will yield effectively the same filter.

B. Multiple Hypothesis Formulation

Given knowledge of the K symbols at the destination receiver, the $K+1$ hypothesis formulation (including the null hypothesis) can be expressed as

$$\begin{aligned} \mathcal{H}_0 &: \quad \mathbf{y} = \mathbf{S}\mathbf{x} + \mathbf{u} \\ \mathcal{H}_k &: \quad \mathbf{y} = \mathbf{S}\mathbf{x} + \alpha \mathbf{c}_k + \mathbf{u} \quad \text{for} \quad k = 1,\ 2,\ \cdots,\ K. \end{aligned} \tag{17}$$

The occurrence of a partial symbol within the observation interval is considered as an occurrence of the null hypothesis by the argument that the lack of coherent integration of the symbol via receive filtering on this interval will cause it to be negligible with respect to the clutter term. Ignoring the null hypothesis for the moment and under the assumption that the K possible symbols are equally likely, it is clear that an intermediate detection metric is

$$\left| z_{y,\max}^{(k)} \right| \;=\; \max_{j,\,\ell} \; |z_{y,j}(\ell)| \tag{18}$$

which is the maximum response across all K symbols over the observation interval with

$$k \;=\; \arg\max_{j,\,\ell} \; |z_{y,j}(\ell)| \ . \tag{19}$$

To provide a low probability of intercept, the embedded symbol has much lower power than the clutter. This condition complicates the detection of the correct symbol because residual clutter may remain after interference cancellation. The inclusion of the null hypothesis provides a means to minimize the detection of false symbols by establishing a symbol-free baseline for the residual interference and noise. In so doing, the symbol detector can monitor for the presence of an embedded symbol without the need for prior cueing or synchronization. As such we consider a second detector stage where the second set of hypotheses is defined as

$$\begin{aligned} \widetilde{\mathcal{H}}_0 :& \quad z_y = z_x + z_u \\ \widetilde{\mathcal{H}}_1 :& \quad z_y = z_x + \alpha\Delta + z_u \end{aligned} \tag{20}$$

which follows from the first stage of interference cancellation filtering where z_x corresponds to the residual clutter after filtering and z_u is the filtered noise. Because only one (or none) of the K symbols can be present within the observation interval, hypothesis $\widetilde{\mathcal{H}}_1$ corresponds to the case when one of the receive filters matches the embedded symbol thus resulting in a processing gain of Δ which is analytically derived in Section IV-C. All other cases (including the application of the other $K-1$ filters) fall under the $\widetilde{\mathcal{H}}_0$ hypothesis.

Because the signal strength α is not known to the destination receiver, we shall rely on the Neyman-Pearson criterion. While the distribution of the random scattering in $x(t)$ is not known, if it is assumed to be zero-mean then the linear transformation $\mathbf{Sx}$ from (17) followed by the filtering operation $\mathbf{w}_j^H \mathbf{y}$ will cause the values of $z_{y,j}(\ell)$ for $j \neq k$ under the null hypothesis to tend to a zero-mean complex Gaussian distribution via the central limit theorem. Thus, since the subsequent pdf of $|z_y|$ for $\widetilde{\mathcal{H}}_0$ is a Rayleigh distribution, it is easily shown that the Neyman-Pearson threshold [16] is computed as

$$\mathcal{T} = \sqrt{-2\sigma_0^2 \, \ln P_{\text{fa}}} \tag{21}$$

where P_{fa} is the desired false alarm rate and σ_0^2 is the variance of $z_{y,j}(\ell)$ for $j \neq k$ and $\forall \ell$. Thus the overall detector output is

$$\text{symbol decision} = \begin{cases} k^{\text{th}} \text{ symbol}, & \text{if } z_{y,\max}^{(k)} > \mathcal{T} \\ \text{no symbol}, & \text{otherwise} \end{cases} . \tag{22}$$

C. Processing Gain

For traditional spread-spectrum communications the processing gain is the time-bandwidth product of the signal. However, because the filter here must also perform interference cancellation on the radar clutter, such is not the case for the processing gain Δ from $\widetilde{\mathcal{H}}_1$ in (20). To assess the processing gain we shall compare the signal-to-interference-plus-noise ratio before $(\mathrm{SINR_i})$ and after receive filtering $(\mathrm{SINR_o})$.

This analysis assumes the absence of mismatch between the tag and destination receiver symbol sets and also assumes that the clutter and noise are complex Gaussian with distributions $\mathbf{x} \sim \mathcal{CN}\left(\mathbf{0}, \sigma_x^2 \mathbf{I}\right)$ for σ_x^2 the clutter power and $\mathbf{u} \sim \mathcal{CN}\left(\mathbf{0}, \sigma_u^2 \mathbf{I}\right)$ for σ_u^2 the noise power. Without loss of generality the discretized radar waveform $\mathbf{s}$ used in (15) and the set of seed vectors $\mathbf{b}_k$ for $k = 1, 2, \cdots, K$ from (6) are defined such that $||\mathbf{s}||^2 = 1$ and $||\mathbf{b}_k||^2 = 1$.

From part A of the Appendix, the $\mathrm{SINR_i}$ is computed by taking the expectation of $||\mathbf{y}||^2$ from (15) which results in

$$\mathrm{SINR_i} = \frac{|\alpha|^2 \left(\frac{NM-m}{NM}\right)}{\sigma_x^2\, NM \; + \; \sigma_u^2\, NM} \, . \tag{23}$$

For the filtered output we compute $\mathrm{SINR_o}$ by taking the expectation of $|\mathbf{w}_k^H \mathbf{y}|^2$ which, according to part B of the Appendix, yields

$$\mathrm{SINR_o} = \frac{|\alpha|^2 \, (NM-m)^2}{NM \left(\sigma_x^2 \, \mathrm{tr}\{\mathbf{\Lambda}_{\mathrm{ND}}\} \; + \; \sigma_u^2 \, (NM-m)\right)} \tag{24}$$

where $\mathrm{tr}\{\cdot\}$ is the matrix trace operation.

The ratio of (24) and (23) results in the processing gain as a function of m:

$$\Delta(m) = \frac{\mathrm{SINR_o}}{\mathrm{SINR_i}} = \frac{(NM-m)\left(\sigma_x^2\, NM \; + \; \sigma_u^2\, NM\right)}{\sigma_x^2 \, \mathrm{tr}\{\mathbf{\Lambda}_{\mathrm{ND}}\} \; + \; \sigma_u^2 \, (NM-m)} \, . \tag{25}$$

Using the fact that $\mathrm{tr}\{\mathbf{\Lambda}_{\mathrm{ND}}\} \leq \lambda_{m+1} \, (NM-m)$, for λ_{m+1} the largest non-dominant eigenvalue, we can simplify (25) as

$$\Delta(m) \geq NM \left(\frac{\sigma_x^2 \; + \; \sigma_u^2}{\sigma_x^2 \, \lambda_{m+1} \; + \; \sigma_u^2}\right) \, . \tag{26}$$

If the noise dominates the radar clutter at the receiver then (26) reduces to $\Delta \approx NM$ which is the expected coherent integration gain for a signal in noise alone. More interesting, though, is the case in which the clutter dominates such that (26) reduces to $\Delta \approx NM\lambda_{m+1}^{-1}$ where $\lambda_{m+1}^{-1} \gg 1$ as m exceeds much beyond N due to the concentration of the clutter power in the N largest eigenvalues. For example, using $NM = 200$ with a dominant subspace rank of $m = N = 100$, the same waveform employed for Figure 3, and a clutter-to-noise ratio (CNR) of $\sigma_x^2/\sigma_u^2 = 30$ dB, the processing gain in (26) is found to be $\Delta = 26.4$ dB which is more than double the coherent integration gain of $NM = 23$ dB. Thus the processing gain Δ may significantly exceed the coherent integration gain. Figure 5 illustrates that the processing gain may even be orders of magnitude greater than the integration gain. This result is due to the fact that the processing gain is the combined response from both coherent integration and interference cancellation.

V. Intercept Metric

An intercept receiver may observe the radar waveform $\mathbf{s}$ as well as the signal in (15) but is not privy to the symbols $\mathbf{c}_k$. If the intercept receiver is searching for an embedded symbol of the type discussed here then it would need to suppress the interference in (15) and then scan for residual energy that stands out from the background. This intercept metric can be expressed as

$$\mathcal{E}_{\rm ir}(n,\ell) = \mathbf{y}^H(\ell)\ \mathbf{P}_n\, \mathbf{y}(\ell) \tag{27}$$

where the projection matrix is

$$\mathbf{P}_n = \mathbf{I} - \mathbf{V}_{{\rm D},n}\mathbf{V}_{{\rm D},n}^H = \mathbf{V}_{{\rm ND},n}\mathbf{V}_{{\rm ND},n}^H \tag{28}$$

with $\mathbf{V}_{{\rm D},n}$ and $\mathbf{V}_{{\rm ND},n}$ the dominant and non-dominant subspaces of rank n and $NM - n$, respectively, employed by the intercept receiver to search the different interference residue subspaces by varying n over the integers in $[0, NM-1]$. Note that unlike the destination receiver, (27) relies solely on interference cancellation (without the benefit of coherent symbol integration). Defining $\mathcal{T}_{\rm ir}(n)$ as the intercept metric threshold as a function of n and $\mathcal{E}_{\rm ir,max}(n) = \max\{\mathcal{E}_{\rm ir}(n,\ell)\}$ over ℓ for each n, then an intercept detection can be declared according to

$$\mathcal{E}_{\rm ir,max}(n) \ \underset{<}{\overset{>}{}}\ \mathcal{T}_{\rm ir}(n)\ . \tag{29}$$

Applying the central limit theorem as before, it can be shown that $\mathcal{E}_{\rm ir}(n,\ell)$ is distributed as the sum of $NM-n$ independent exponential distributions, the individual rates of which are the diagonal elements of $\left[\sigma_x^2 \mathbf{\Lambda}_{{\rm ND},n} + \sigma_u^2 \mathbf{I}_{(NM-n)}\right]$ from part C of the Appendix. Thus the desired false alarm probability can be computed to determine the subsequent threshold $\mathcal{T}_{\rm ir}(n)$.

To facilitate analysis of the intercept metric in (27) we make the assumption that the intercept receiver has clairvoyant knowledge of the symbol dimensionality NM (in light of this assumption the subsequent analysis can be considered a theoretical worst-case scenario with respect to LPI). Under the presumption that the signal interval of $\mathbf{y}$ containing radar clutter may also contain an unknown embedded symbol, the logical solution is to suppress the clutter interference and then attempt to detect signal energy against the background of noise and residual interference.

We can compute the intercept receiver $\mathrm{SINR}_{\mathrm{ir}}$ by evaluating the components of

$$\mathcal{E}_{\mathrm{ir}} = E\left[\mathbf{y}^H \mathbf{P}_n \, \mathbf{y}\right] = E\left[\mathbf{x}^H \mathbf{S}^H \mathbf{P}_n \, \mathbf{S}\mathbf{x}\right] + E\left[\mathbf{u}^H \mathbf{P}_n \, \mathbf{u}\right] + |\alpha|^2 \, \mathbf{c}_k^H \mathbf{P}_n \, \mathbf{c}_k \tag{30}$$

where we have again invoked independence between the symbol, clutter, and noise. As derived in part C of the Appendix,

$$\mathrm{SINR}_{\mathrm{ir}} = \frac{|\alpha|^2 \left(\frac{NM - \max\{m,n\}}{NM}\right)}{\sigma_x^2 \, \mathrm{tr}\{\mathbf{\Lambda}_{\mathrm{ND},n}\} \; + \; \sigma_u^2 \, (NM - n)} \; . \tag{31}$$

Using (31), we can define two additional performance metrics. The first of these is the intercept receiver gain $\Delta_{\mathrm{ir}}(n;m)$ which is a function of n for a given value of m and is defined as

$$\Delta_{\mathrm{ir}}(n;m) = \frac{\mathrm{SINR}_{\mathrm{ir}}}{\mathrm{SINR}_{\mathrm{i}}} = \frac{(NM - \max\{m,n\}) \, (\sigma_x^2 NM \; + \; \sigma_u^2 NM)}{(NM - m) \, (\sigma_x^2 \, \mathrm{tr}\{\mathbf{\Lambda}_{\mathrm{ND},n}\} \; + \; \sigma_u^2 (NM - n))} \; . \tag{32}$$

Comparing the destination receiver gain from (26) with the intercept receiver gain of (32) we can also define the "gain advantage" Ψ due to coherent integration in the destination receiver as

$$\Psi(m,n) = \frac{\Delta_{\mathrm{i}}(m)}{\Delta_{\mathrm{ir}}(n;m)} = \frac{(NM - m)^2 \, (\sigma_x^2 \, \mathrm{tr}\{\mathbf{\Lambda}_{\mathrm{ND},n}\} \; + \; \sigma_u^2 \, (NM - n))}{(NM - \max\{m,n\}) \, (\sigma_x^2 \, \mathrm{tr}\{\mathbf{\Lambda}_{\mathrm{ND}}\} \; + \; \sigma_u^2 \, (NM - m))} \tag{33}$$

which, after again employing $\mathrm{tr}\{\mathbf{\Lambda}_{\mathrm{ND}}\} \leq \lambda_{m+1} \, (NM - m)$, reduces to

$$\Psi(m,n) \geq \left(\frac{NM - m}{NM - \max\{m,n\}}\right) \left(\frac{\sigma_x^2 \, \mathrm{tr}\{\mathbf{\Lambda}_{\mathrm{ND},n}\} \; + \; \sigma_u^2 \, (NM - n)}{\sigma_x^2 \, \lambda_{m+1} \; + \; \sigma_u^2}\right) \; . \tag{34}$$

Because Ψ is a function of m for all values of n that the intercept receiver could employ, (34) provides a means for the tag and destination receiver to optimize the dimensionality of the non-dominant subspace for a given N, M, and radar waveform $\mathbf{s}$ to obtain a desired number of symbols K while ensuring the gain advantage is preserved. This goal can be accomplished by performing the maximin optimization

$$\max_m \min_n \Psi(m,n) \tag{35}$$

under the constraint $(NM - m) \geq K$. This problem can be solved empirically through evaluation of the $(NM)^2$ possible combinations of m and n. Returning to the example of an LFM radar waveform with $N = 100$, $M = 2$, and clutter-to-noise ratio (CNR) $= 30$ dB, Figure 6 illustrates $\Psi(m,n)$ where the value of $m = 157$ is found to solve the maximin problem in (35). Actually, values in $150 \leq m \leq 165$ all yield similar values of $\Psi(m,n)$ with respect to n of ~ 14.5 dB.

VI. Simulated Performance

To assess the performance of the proposed intra-pulse radar-embedded communication paradigm we shall use the LFM radar waveform with $N = 200$, $M = 2$, and CNR $= 30$ dB. From the analysis above, we set $m = 160$. For $K = 16$ symbols, $\log_2 K = 4$ bits are transmitted in the backscatter of each radar pulse. Note that, because of the way the symbols are defined, they are all equidistant from one another such that the mapping of bits to each symbol is arbitrary (no "nearest neighbor" to exploit). To contrast the performance between the destination receiver and the intercept receiver the result are shown in terms of received SNR with the communications standard measure obtained as $E_b/N_0 = \mathrm{SNR} + 17$ dB.

To simulate the continuous nature of reality all discrete sequences (for example $\mathbf{s}$ and $\mathbf{c}_k$) are up-sampled by an additional factor of 7. Channel effects such as multipath and clutter occur at this "continuous" sampling rate. The tag, destination receiver, and intercept receiver each apply low-pass filtering and down-sampling to obtain the MN "discrete" sampling rate. Each multipath channel is independently drawn and is modeled with 10 impulses including a direct path component and 9 multipath components randomly distributed over $[0, T/2]$, for T the radar pulse width. Each impulse is multiplied by a value drawn from a complex Gaussian distribution to randomize amplitude and phase.

At both the tag and destination receiver (if not the radar), for the purpose of determining the K symbols the incident radar illumination $\widetilde{s}(t)$ is employed (*i.e.* no *a priori* knowledge of the radar waveform). This is done to exemplify the robustness of symbol determination between the tag and destination receiver. That said, when time reversal is to be employed the actual radar waveform $s(t)$ is assumed known by the tag to enable non-blind channel estimation. Because the radar transmits at a high power to contend with two-way path loss the SNR of the radar illumination incident upon the tag and destination receiver is set to 30 dB.

A. BER Performance

Figure 7 depicts the BER performance after applying the set of K filters $\mathbf{w}_k$ and selecting the symbol associated with the maximum $|z_{y,j}(\ell)|$ over ℓ and for $j \in [1, K]$. Results are shown for the case when a) no multipath is present, b) multipath distorts the received symbol, and c) the tag estimates the multipath and uses time-reversal. Because this communication paradigm does not involve inter-symbol interference it is observed that multipath has a rather minor impact on

BER performance. The performance gain from the use of time-reversal is significant, though, due to spatio-temporal focusing at the radar receiver.

With the Neyman-Pearson (NP) detection stage included, a detector BER can be defined as

$$\mathrm{BER}_{\mathrm{det}} = \frac{\text{number of incorrect symbols detected}}{\text{total number of symbols}} \tag{36}$$

with the related probability of symbol detection denoted as

$$P_{\mathrm{det}} = \frac{\text{number of correct symbols detected}}{\text{total number of symbols}} \tag{37}$$

and the probability of not detecting a correct symbol (from the receive filtering stage) as

$$P_{\mathrm{miss}} = \frac{\text{number of correct symbols not detected}}{\text{number of correct symbols}}. \tag{38}$$

Figure 8 shows the BER results for the NP detector using $P_{\mathrm{fa}} = 10^{-5}$ where it is observed that the highest BER values are $\approx 10^{-2}$ since incorrect symbols are less likely to pass the detector.

The related measures from (37) and (38) are shown in Figures 9 and 10, respectively. It is the detection probability in Figure 9 that serves to maintain the low BER values shown in Figure 8 for low values of SNR. In contrast, Figure 10 captures the amount of lost correct symbols due to the use of the NP detector which is the price paid for confidence in the symbol decisions.

B. Probability of Intercept

To assess the probability of intercept (P_{int}) we consider the intercept metric (27). The threshold in (29) is computed numerically from the pdf of $\mathcal{E}_{\mathrm{ir}}$ to provide a theoretical $P_{\mathrm{fa}} = 10^{-5}$. The intercept probability is then determined by performing 10,000 trials for each SNR value in which an intercept detection is declared if $\mathcal{E}_{\mathrm{ir,max}}(n)$ exceeds the associated threshold $\mathcal{T}_{\mathrm{ir}}(n)$ for any value of n. The probability of intercept is depicted in Figure 9 where it is observed that, as a function of SNR, P_{det} (detection probability for the destination receiver) with or without multipath present is approximately 5 dB better than P_{int}. Furthermore, when the ta uses time-reversal P_{det} is found to be approximately 10 dB better than P_{int}. Given that this intercept metric employs clairvoyant knowledge and thus considered a worst case in terms of LPI, it can be surmised that the proposed radar-embedded communication scheme does demonstrate good potential for covert communications.

VII. Conclusions

A new form of covert communication has been presented that relies upon the interference from a pulsed radar system to hide in the resulting backscatter. Communication symbols are adaptively determined as a function of the radar illumination and have been shown to be robust to multipath effects. Also, this new paradigm can naturally exploit time-reversal as a means to achieve spatio-temporal focusing if the destination communication receiver is the illuminating radar. Based on analytical assessment of the received signal containing the embedded symbol, the processing gain of the new communication paradigm has been shown to exceed the standard coherent integration gain for spread spectrum communications due to the inclusion of interference cancellation effects. The processing gain for the intercept receiver is obtained through a similar analysis with the ratio of the two processing gains revealing the "gain advantage" as a metric that can be optimized for design parameterization of the covert symbols.

References

[1] S. D. Blunt, P. Yatham, and J. Stiles, "Intra-pulse radar embedded communications," *IEEE Trans. Aerospace and Electronic Systems*, vol. 46, no. 3, pp. 1185-1200, July 2010.

[2] D.D. Mawhinney, "Microwave tag identification systems," *RCA Review*, vol. 44, no. 4, pp. 589-610, Dec. 1983.

[3] S.D. Koelle, S.W. Depp, and R.W. Freyman, "Short-range radio-telemetry for electronic identification, using modulated RF backscatter," *Proc. IEEE*, vol. 63, no, 8, pp. 1260-1261, Aug. 1975.

[4] D. L. Nicholson, *Spread Spectrum Signal Design: Low Probability of Exploitation and Anti-Jam Systems*, Freeman, San Francisco, 1988.

[5] D. Hounam and K.H. Wagel, "A technique for the identification and localization of SAR targets using encoding transponders," *IEEE Trans. Geoscience and Remote Sensing*, vol. 39, no. 1, pp. 3-7, Jan. 2001.

[6] M. Onoe, N. Hasebe, and T. Zamas, "Radar reflectors with controllable reflection", *Electronics and Communications in Japan, Part I: Communications*, vol. 63, no. 3, pp. 51-58, Mar. 1980.

[7] B.H. Cantrell, J.O. Coleman, and G.V. Trunk, "Radar Communications," *Naval Research Lab Report 8515*, 1991.

[8] Z. Hijaz and V.S. Frost, "Exploiting OFDM systems for covert communication," *IEEE Military Communications Conf.*, 2010.

[9] H. Stockman, "Communication by means of reflected power," *Proc. IRE*, vol. 36, no. 10, pp. 1196-1204, Oct. 1948.

[10] N. Levanon and E. Mozeson, *Radar Signals*, IEEE Press, 2004.

[11] M. Skolnik, *Introduction to Radar Systems, 3rd ed.*, McGraw-Hill, 2001.

[12] A. Derode, A. Tourin, J. de Rosny, M. Tanter, S. Yon, and M. Fink, "Taking Advantage of Multiple Scattering to Communicate with Time-Reversal Antennas," *Phys. Rev. Lett.*, vol. 90, no. 1, p. 014301, Jan. 2003.

[13] M. Soumekh, "SAR-ECCM using phase-perturbed LFM chirp signals and DRFM repeat jammer penalization," *IEEE Trans. Aerospace and Electronic Systems*, vol. 42, no. 1, pp. 191-205, Jan. 2006.

[14] R. Lupas and S. Verdu, "Linear multiuser detectors for synchronous code-division multiple-access channels," *IEEE Trans. Information Theory*, vol. 35, no. 1, pp. 123-136, Jan. 1989.

[15] S. Verdu, S, *Multiuser Detection*, Cambridge University Press, Cambridge, UK, 1998.

[16] S. Kay, *Fundamentals of Statistical Signal Processing: Detection Theory*, Prentice Hall, 1998.

VIII. Appendix

A. $SINR_i$

Assuming statistical independence between the clutter, noise, and the deterministic k^{th} embedded symbol, the expectation of $||\mathbf{y}||^2$ yields

$$E\left[\mathbf{y}^H\mathbf{y}\right] = E\left[\mathbf{x}^H\mathbf{S}^H\mathbf{S}\mathbf{x}\right] + E\left[\mathbf{u}^H\mathbf{u}\right] + |\alpha|^2\,\mathbf{c}_k^H\mathbf{c}_k\ . \tag{39}$$

The first term in (39) corresponds to the clutter and can be decomposed as

$$\begin{aligned} E\left[\mathbf{x}^H\mathbf{S}^H\mathbf{S}\mathbf{x}\right] &= E\left[\ \mathrm{tr}\left\{\mathbf{S}^H\mathbf{S}\mathbf{x}\mathbf{x}^H\right\}\right] \\ &= \sigma_x^2\ \mathrm{tr}\left\{\mathbf{S}\mathbf{S}^H\right\} \\ &= \sigma_x^2\ NM \end{aligned} \tag{40}$$

since the diagonal elements of $\mathbf{S}\mathbf{S}^H$ are unity due to $||\mathbf{s}||^2 = 1$ and $\mathrm{tr}\{\cdot\}$ is the matrix trace operation. The second term in (39) corresponds to the noise and can be expressed as

$$\begin{aligned} E\left[\mathbf{u}^H\mathbf{u}\right] &= E\left[\ \mathrm{tr}\left\{\mathbf{u}\mathbf{u}^H\right\}\right] \\ &= \sigma_u^2\ NM\ . \end{aligned} \tag{41}$$

Finally, the third term in (39) corresponds to the embedded symbol and can be decomposed as

$$\begin{aligned} |\alpha|^2\,\mathbf{c}_k^H\mathbf{c}_k &= |\alpha|^2\,\mathbf{b}_k^H\mathbf{V}_{\mathrm{ND}}\mathbf{V}_{\mathrm{ND}}^H\mathbf{V}_{\mathrm{ND}}\mathbf{V}_{\mathrm{ND}}^H\mathbf{b}_k \\ &= |\alpha|^2\,\mathbf{b}_k^H\mathbf{V}_{\mathrm{ND}}\mathbf{V}_{\mathrm{ND}}^H\mathbf{b}_k \\ &= |\alpha|^2\,\mathbf{q}_k^H\mathbf{q}_k \end{aligned} \tag{42}$$

where $\mathbf{q}_k = \mathbf{V}_{\mathrm{ND}}^H\mathbf{b}_k$ is an $(NM - m)\times 1$ vector that will also arise in the analysis of the filtered output $\mathrm{SINR}_{\mathrm{o}}$. Because $\mathbf{b}_k$ has length NM and $||\mathbf{b}_k||^2 = 1$ we can define an average element value as $|b_{k,i}|^2_{\mathrm{avg}} = \frac{1}{NM}$ which likewise translates to $|q_{k,i}|^2_{\mathrm{avg}} = \frac{1}{NM}$ by the unitary nature of $\mathbf{V}$. Hence (42) simplifies to

$$|\alpha|^2\,\mathbf{c}_k^H\mathbf{c}_k\ =\ |\alpha|^2\left(\frac{NM - m}{NM}\right)\ . \tag{43}$$

Combining (40), (41), and (43) yields the input SINR in (23).

B. $SINR_o$

Again assuming statistical independence between the clutter, noise, and the embedded symbol, the expectation of the output power is

$$E\left[|\mathbf{w}_k^H \mathbf{y}|^2\right] = E\left[\mathbf{w}_k^H \mathbf{S}\mathbf{x}\mathbf{x}^H \mathbf{S}^H \mathbf{w}_k\right] \;+\; E\left[\mathbf{w}_k^H \mathbf{u}\mathbf{u}^H \mathbf{w}_k\right] \;+\; |\alpha|^2\, \mathbf{w}_k^H \mathbf{c}_k\, \mathbf{c}_k^H \mathbf{w}_k\ . \tag{44}$$

To evaluate the terms in (44), we first decompose the receive filter in (16) as

$$\begin{aligned} \mathbf{w}_k &= \left(\mathbf{S}\mathbf{S}^H + \delta\mathbf{I}\right)^{-1} \mathbf{c}_k \\ &= \left(\mathbf{V}\boldsymbol{\Lambda}\mathbf{V}^H + \delta\mathbf{I}\right)^{-1} \mathbf{c}_k \\ &= \mathbf{V}\left(\boldsymbol{\Lambda} + \delta\mathbf{I}\right)^{-1} \mathbf{V}^H\, \mathbf{V}_{\text{ND}}\, \mathbf{V}_{\text{ND}}^H\, \mathbf{b}_k \\ &= \mathbf{V}_{\text{ND}}\left(\boldsymbol{\Lambda}_{\text{ND}} + \delta\mathbf{I}\right)^{-1}\ \mathbf{V}_{\text{ND}}^H\, \mathbf{b}_k \\ &\cong \delta^{-1}\mathbf{V}_{\text{ND}}\, \mathbf{V}_{\text{ND}}^H\, \mathbf{b}_k \end{aligned} \tag{45}$$

where we have made use of the definition in (7) and the approximation $\left(\boldsymbol{\Lambda}_{\text{ND}} + \delta\mathbf{I}\right)^{-1} \cong \delta^{-1}\mathbf{I}$ with $\boldsymbol{\Lambda}_{\text{ND}}$ the diagonal matrix of the $NM - m$ non-dominant eigenvalues, the largest of which is equal to δ. The result in (45) could also be obtained without a loading factor by using $\left(\mathbf{V}\widetilde{\boldsymbol{\Lambda}}\mathbf{V}^H\right)^{-1}$ in (16) where $\widetilde{\boldsymbol{\Lambda}}$ has the $NM - m$ non-dominant eigenvalues set to δ.

Using the result of (45), the clutter term in (44) can be decomposed as

$$\begin{aligned} E\left[\mathbf{w}_k^H \mathbf{S}\mathbf{x}\mathbf{x}^H \mathbf{S}^H \mathbf{w}_k\right] &= \delta^{-2}\, \mathbf{b}_k^H \mathbf{V}_{\text{ND}} \mathbf{V}_{\text{ND}}^H \mathbf{S}\ E\left[\mathbf{x}\mathbf{x}^H\right] \mathbf{S}^H \mathbf{V}_{\text{ND}} \mathbf{V}_{\text{ND}}^H \mathbf{b}_k \\ &= \sigma_x^2\, \delta^{-2}\, \mathbf{b}_k^H \mathbf{V}_{\text{ND}} \mathbf{V}_{\text{ND}}^H \mathbf{S}\mathbf{S}^H \mathbf{V}_{\text{ND}} \mathbf{V}_{\text{ND}}^H \mathbf{b}_k \\ &= \sigma_x^2\, \delta^{-2}\, \mathbf{b}_k^H \mathbf{V}_{\text{ND}} \mathbf{V}_{\text{ND}}^H \mathbf{V}\boldsymbol{\Lambda}\mathbf{V}^H \mathbf{V}_{\text{ND}} \mathbf{V}_{\text{ND}}^H \mathbf{b}_k \\ &= \sigma_x^2\, \delta^{-2}\, \mathbf{b}_k^H \mathbf{V}_{\text{ND}} \boldsymbol{\Lambda}_{\text{ND}} \mathbf{V}_{\text{ND}}^H \mathbf{b}_k \\ &= \sigma_x^2\, \delta^{-2}\, \mathbf{q}_k^H \boldsymbol{\Lambda}_{\text{ND}} \mathbf{q}_k \end{aligned} \tag{46}$$

where the last step follows from (42). Again using the average value $|q_{k,i}|^2_{\text{avg}} = \frac{1}{NM}$, the clutter term in (46) can be approximated as

$$E\left[\mathbf{w}_k^H \mathbf{S}\mathbf{x}\mathbf{x}^H \mathbf{S}^H \mathbf{w}_k\right] \cong \frac{\sigma_x^2\, \delta^{-2}\, \operatorname{tr}\{\boldsymbol{\Lambda}_{\text{ND}}\}}{NM}\ . \tag{47}$$

Likewise the noise term in (44) can be decomposed as

$$\begin{aligned} E\left[\mathbf{w}_k^H \mathbf{u}\mathbf{u}^H \mathbf{w}_k\right] &= \delta^{-2}\, \mathbf{b}_k^H \mathbf{V}_{\text{ND}} \mathbf{V}_{\text{ND}}^H\ E\left[\mathbf{u}\mathbf{u}^H\right] \mathbf{V}_{\text{ND}} \mathbf{V}_{\text{ND}}^H \mathbf{b}_k \\ &= \sigma_u^2\, \delta^{-2}\, \mathbf{b}_k^H \mathbf{V}_{\text{ND}} \mathbf{V}_{\text{ND}}^H \mathbf{b}_k \\ &= \sigma_u^2\, \delta^{-2}\, \mathbf{q}_k^H \mathbf{q}_k \\ &= \sigma_u^2\, \delta^{-2}\ \left(\tfrac{NM-m}{NM}\right) \end{aligned} \tag{48}$$

using the result from (42) and (43). Finally, the embedded symbol component of (44) can be expressed as

$$\begin{aligned}
|\alpha|^2 \mathbf{w}_k^H \mathbf{c}_k \mathbf{c}_k^H \mathbf{w}_k &= |\alpha|^2 \, \delta^{-2} \, \left(\mathbf{b}_k^H \mathbf{V}_{\mathrm{ND}} \mathbf{V}_{\mathrm{ND}}^H \mathbf{V}_{\mathrm{ND}} \mathbf{V}_{\mathrm{ND}}^H \mathbf{b}_k\right)^2 \\
&= |\alpha|^2 \, \delta^{-2} \, \left(\mathbf{b}_k^H \mathbf{V}_{\mathrm{ND}} \mathbf{V}_{\mathrm{ND}}^H \mathbf{b}_k\right)^2 \\
&= |\alpha|^2 \, \delta^{-2} \, \left(\mathbf{q}_k^H \mathbf{q}_k\right)^2 \\
&= |\alpha|^2 \, \delta^{-2} \, \left(\tfrac{NM-m}{NM}\right)^2 \; .
\end{aligned} \tag{49}$$

After combining (47), (48), and (49) and canceling like terms the output SINR in (24) is obtained.

C. $SINR_{ir}$

From (30) the clutter term is decomposed as

$$\begin{aligned}
E\left[\mathbf{x}^H \mathbf{S}^H \mathbf{P}_n \, \mathbf{S}\mathbf{x}\right] &= E\left[\mathbf{x}^H \mathbf{S}^H \mathbf{V}_{\mathrm{ND},n} \mathbf{V}_{\mathrm{ND},n}^H \, \mathbf{S}\mathbf{x}\right] \\
&= E\left[\, \mathrm{tr}\left\{\mathbf{S}^H \mathbf{V}_{\mathrm{ND},n} \mathbf{V}_{\mathrm{ND},n}^H \, \mathbf{S}\mathbf{x}\mathbf{x}^H\right\}\right] \\
&= \sigma_x^2 \, \mathrm{tr}\left\{\mathbf{V}_{\mathrm{ND},n} \mathbf{V}_{\mathrm{ND},n}^H \, \mathbf{S}\mathbf{S}^H\right\} \\
&= \sigma_x^2 \, \mathrm{tr}\left\{\mathbf{V}_{\mathrm{ND},n} \mathbf{V}_{\mathrm{ND},n}^H \, \mathbf{V}\boldsymbol{\Lambda}\mathbf{V}^H\right\} \\
&= \sigma_x^2 \, \mathrm{tr}\left\{\mathbf{V}_{\mathrm{ND},n} \, \boldsymbol{\Lambda}_{\mathrm{ND},n} \mathbf{V}_{\mathrm{ND},n}^H \, \right\} \\
&= \sigma_x^2 \, \mathrm{tr}\{\boldsymbol{\Lambda}_{\mathrm{ND},n}\}
\end{aligned} \tag{50}$$

where $\boldsymbol{\Lambda}_{\mathrm{ND},n}$ contains the $NM - n$ non-dominant eigenvalues. Similarly, the noise term from (30) is decomposed as

$$\begin{aligned}
E\left[\mathbf{u}^H \mathbf{P}_n \, \mathbf{u}\right] &= E\left[\mathbf{u}^H \mathbf{V}_{\mathrm{ND},n} \mathbf{V}_{\mathrm{ND},n}^H \, \mathbf{u}\right] \\
&= E\left[\, \mathrm{tr}\left\{\mathbf{V}_{\mathrm{ND},n} \mathbf{V}_{\mathrm{ND},n}^H \, \mathbf{u}\mathbf{u}^H\right\}\right] \\
&= \sigma_u^2 \, \mathrm{tr}\left\{\mathbf{V}_{\mathrm{ND},n}^H \mathbf{V}_{\mathrm{ND},n}\right\} \\
&= \sigma_u^2 \, (NM - n) \; .
\end{aligned} \tag{51}$$

Finally the embedded symbol component in (30) can be decomposed as

$$|\alpha|^2 \, \mathbf{c}_k^H \mathbf{P}_n \, \mathbf{c}_k \;\; = \;\; |\alpha|^2 \, \mathbf{b}_k^H \mathbf{V}_{\mathrm{ND}} \mathbf{V}_{\mathrm{ND}}^H \mathbf{V}_{\mathrm{ND},n} \mathbf{V}_{\mathrm{ND},n}^H \, \mathbf{V}_{\mathrm{ND}} \mathbf{V}_{\mathrm{ND}}^H \mathbf{b}_k \; . \tag{52}$$

The term $\mathbf{V}_{\mathrm{ND}} \mathbf{V}_{\mathrm{ND}}^H \mathbf{V}_{\mathrm{ND},n} \mathbf{V}_{\mathrm{ND},n}^H \, \mathbf{V}_{\mathrm{ND}} \mathbf{V}_{\mathrm{ND}}^H \; = \; \mathbf{I}_{(NM-m)}$ if $n \leq m$, otherwise the first $n - m$ diagonal elements of the identity matrix are replaced with zero. Thus using the result from (43), we can express a general form for (52) as

$$|\alpha|^2 \, \mathbf{c}_k^H \mathbf{P}_n \, \mathbf{c}_k \; = \; |\alpha|^2 \, \left(\frac{NM - \max\{m, n\}}{NM}\right) \; . \tag{53}$$

Combining (50), (51), and (53) yields the intercept receiver $\mathrm{SINR}_{\mathrm{ir}}$ shown in (31).

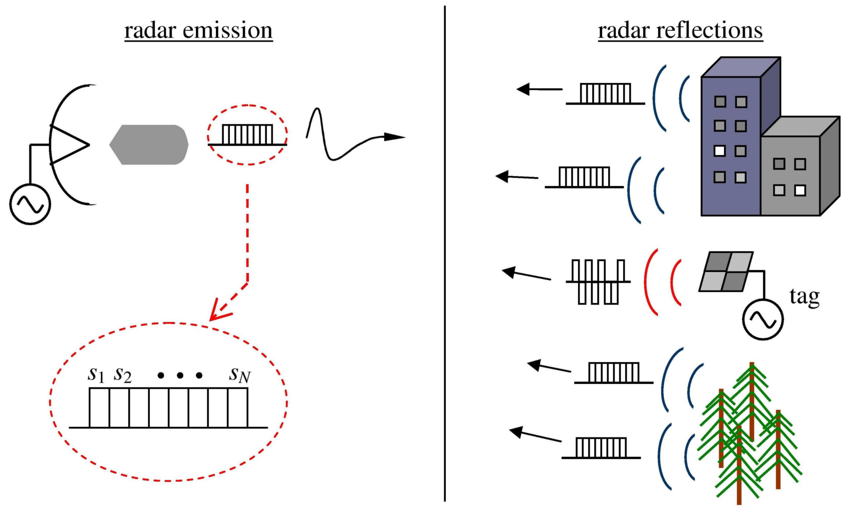

Fig. 1. Covert communication signal embedded in ambient radar scattering

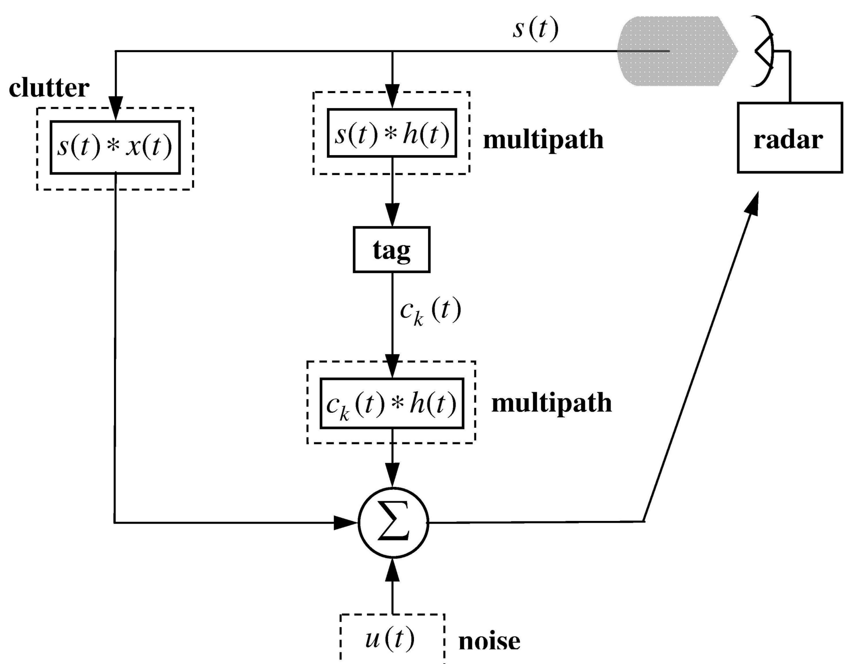

Fig. 2. Overall signal model for intra-pulse communication with the illuminating radar

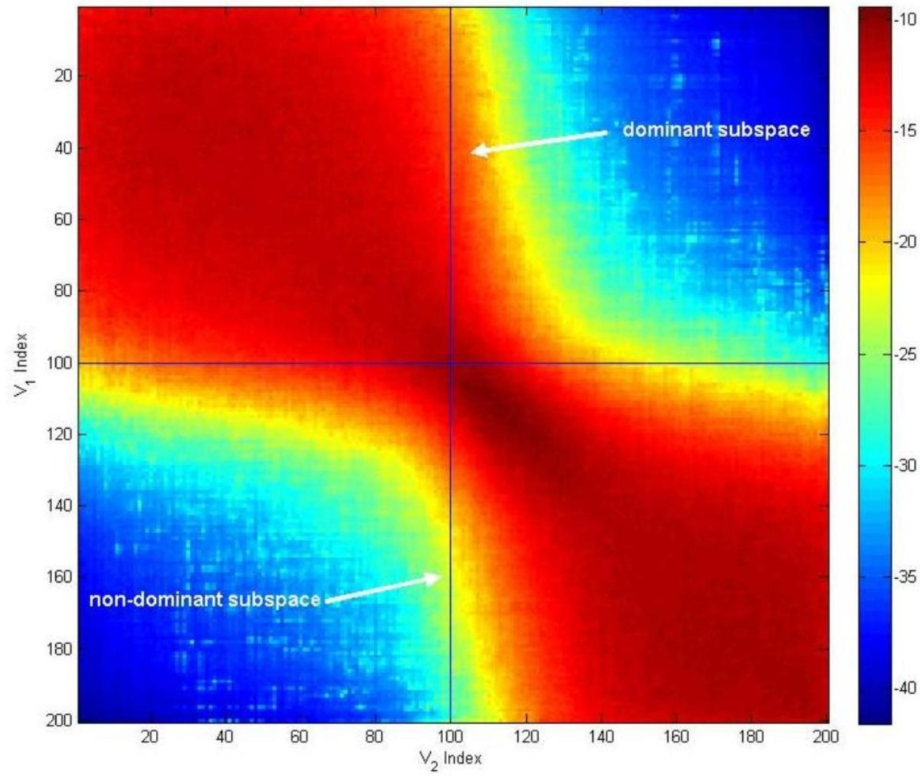

Fig. 3. Average correlation (1000 trials) between eigenvector sets for two independent multipath profiles (dB scale)

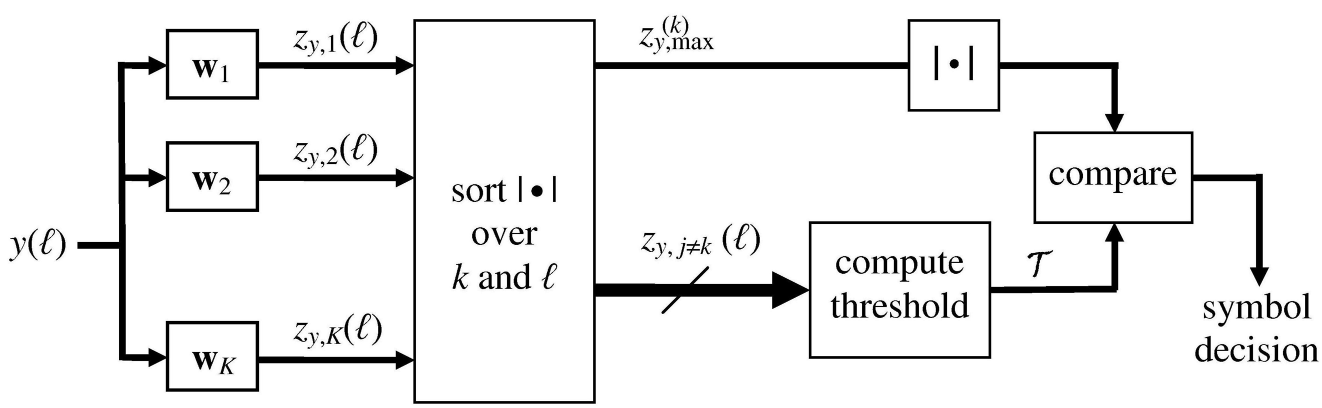

Fig. 4. Signal flow of general decision rule for symbol detection

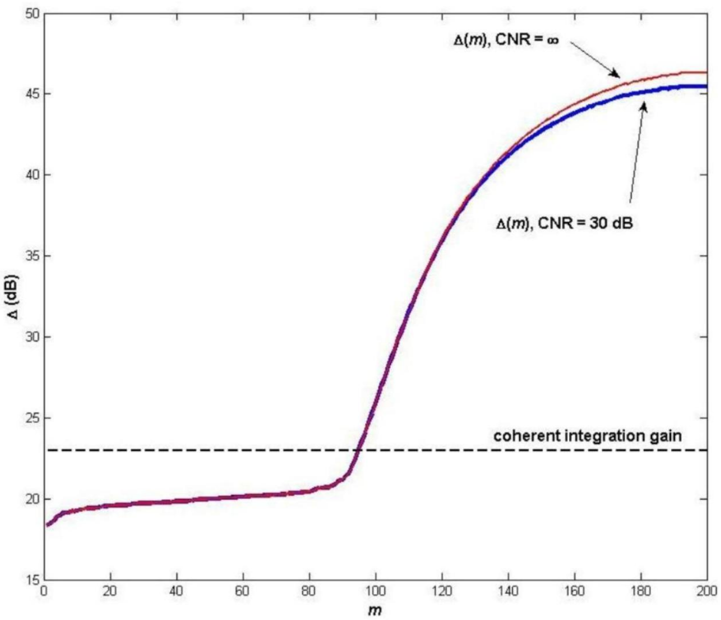

Fig. 5. Processing gain Δ with $NM = 200$ for CNR $= 30$ dB and CNR $= \infty$

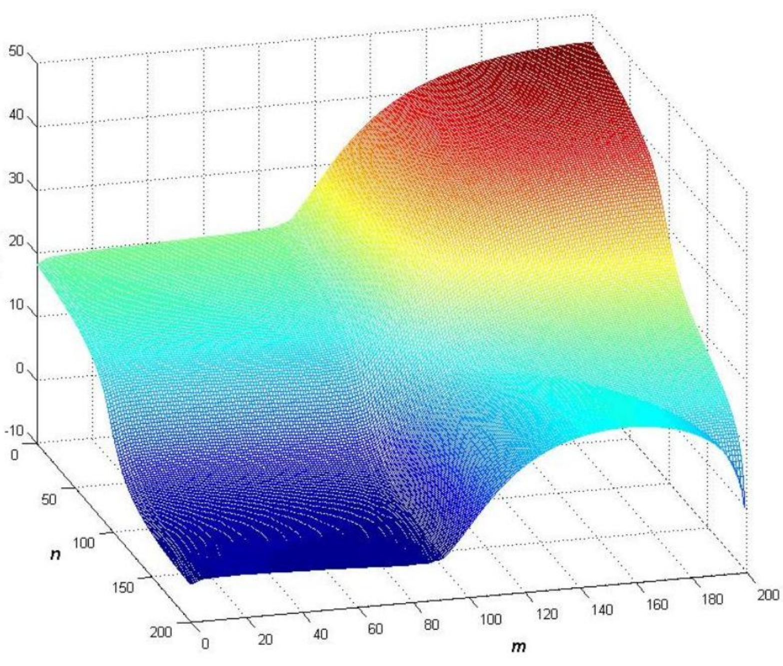

Fig. 6. Gain advantage for $NM = 200$ and CNR $= 30$ dB

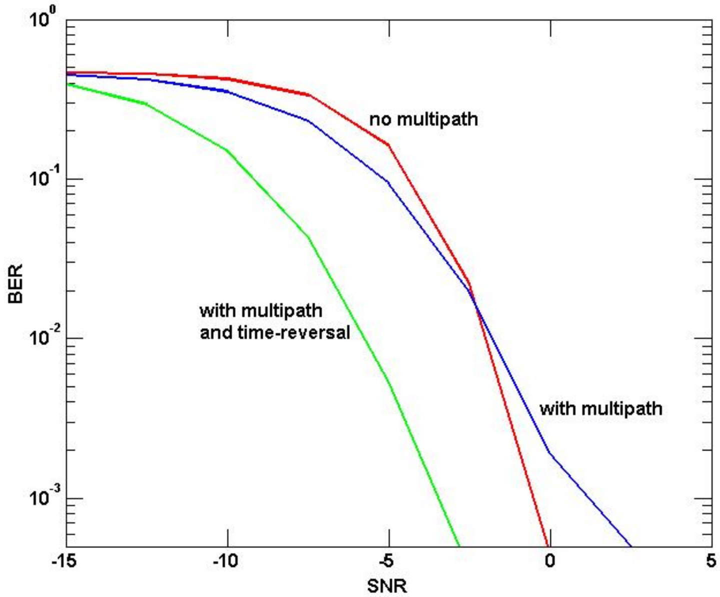

Fig. 7. BER of first-stage symbol selection, $E_b/N_0 = \mathrm{SNR} + 17$ dB

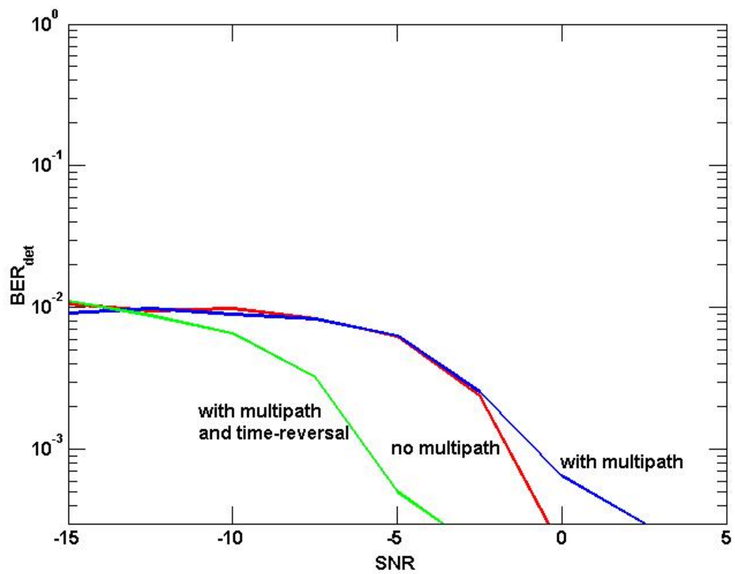

Fig. 8. $\mathrm{BER}_{\mathrm{det}}$ after Neyman-Pearson detector, $E_b/N_0 = \mathrm{SNR} + 17$ dB

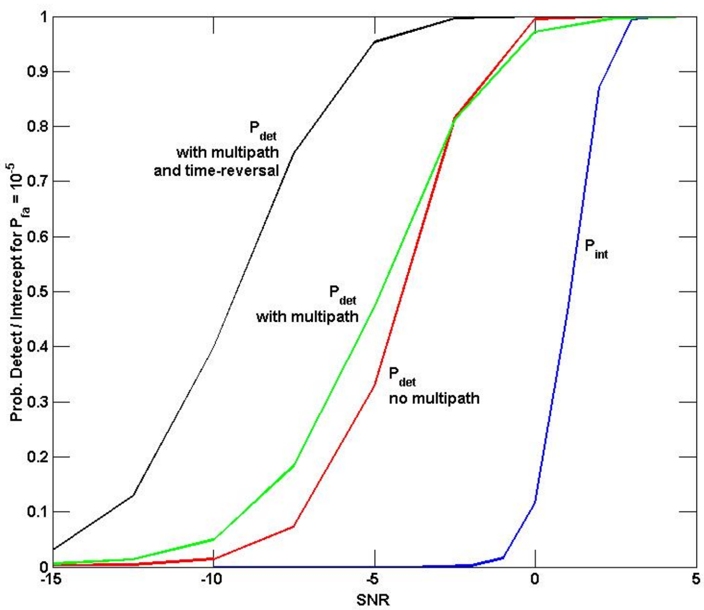

Fig. 9. Probability of symbol detection using the Neyman-Pearson detector

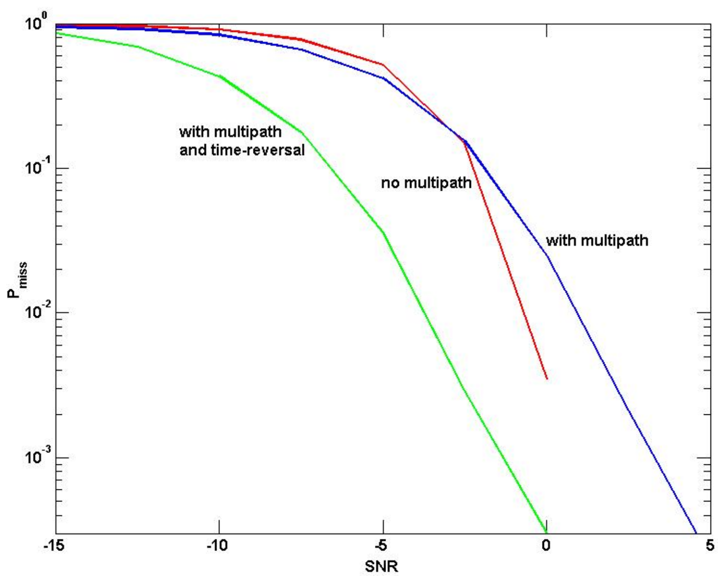

Fig. 10. Probability of not detecting the correctly selected symbol (i.e. $\mathrm{P}_{\mathrm{miss}}$)